Measurement 227 (2024) 114246

Contents lists available at ScienceDirect

Measurement

journal homepage: www.elsevier.com/locate/measurement

On the measurement of the wave power captured by a submerged U-OWC using a temperature sensor

L. Gurnari [a], F. Ruffa [a], M. Lugarà [a], G. Fulco [a], P. Filianoti [b,*]

[a] Department of Information Engineering, Infrastructure and Sustainable Energy (DIIES), University Mediterranea of Reggio Calabria, Via Graziella, 89122 Reggio Calabria, Italy

[b] Department of Civil, Energy, Environmental and Material Engineering (DICEAM), University Mediterranea of Reggio Calabria, Via Graziella, 89122 Reggio Calabria, Italy

ARTICLE INFO

Keywords:
U-OWC
Temperature fluctuation
Captured energy
Thermocouple
CFD

ABSTRACT

To calculate the amount of wave energy captured by an oscillating water column (OWC) converter, we need to measure some fluid dynamic quantities, like pressure and discharge fluctuations, along the fluid motion. In general, direct measurements of the particle velocity is a complicated matter, especially on OWCs provided by a U-duct, in which the presence of the velocity sensor disturbs the motion field. A method to evaluate the energy captured by the plant, by measuring pressure and temperature of the air inside the plenum chamber is here investigated. In this work, we have analyzed the performance of the measurement technique, investigating the influence of the time response of the temperature sensor, through a numerical experiment, using the CFD. We have observed that the measurement of the captured power is strongly affected by the time response of the sensor. Therefore, we have designed a measurement optimization technique which actively corrects the temperature measurements, compensating for the errors in the estimation of the energy flux, due to insufficient response time.

1. Introduction

In recent decades a huge effort has been dedicated to the development and optimization of technologies for the production of electrical energy from renewable sources. Among the many solutions investigated, one of the most interesting is the possibility to use sea waves energy to produce electricity in an economically sustainable way [1]. Wave energy is an unlimited source and, for this reason, it covers an important role for achieving renewable energy goals, by transformation of the kinetic energy of the waves into electric energy [2]. To convert the energy of the motion of the waves into electricity, devices called Wave Energy Converter (WEC) are used. There are many WEC devices, either already built and mounted at sea and also others, more innovative, still under development and research. They can be classified according to the position, with respect to the coast in which they are installed, the position with respect to the motion of the waves, and according to their operating principle [3].

The OWC systems, which use the motion of the wave to produce energy, consist of a reinforced concrete or steel structure. The structure of an OWC consists of a partially submerged chamber, with an opening under the waterline from which the water enters and compresses the air that remains in the upper part of the chamber. The air, then leaves the chamber, passing through a turbine, used to produce electricity [4]. When the water level drops, air enters the chamber from the atmosphere and flows in the opposite direction through the turbine. As a result, low-pressure Wells turbines are often used in these types of systems, which rotate in the same direction regardless of the airflow direction, eliminating the need for airflow rectification [5].

The OWC systems are the most widely studied systems to convert sea wave energy. Among their advantages there are simplicity and robustness [6]. Currently there are many implementations of OWC systems under development with demonstration applications in different countries and, in some cases, even connected to the electricity grid. Among the many systems, the most important devices, which are in the prototype phase or installed are: ”OSPREY” in U.K. [7], ”Pico” [8] and ”Duoro” in Portugal, ”LIMPET” in Scotland [9], ”Sakata” in Japan [10], ”Mutriku” in Spain [11], ”Mighty Whole” in Japan [12], and ”U-OWC” in Italy [13–18]. The latter, also known as U-OWC, gets its name from its shape, which enables the system to harness wave energy without allowing direct entry of waves into the structure. This way, the waves act as an external force with higher efficiency [13]. In this work we

* Corresponding author.
E-mail addresses: luana.gurnari@unirc.it (L. Gurnari), filippo.ruffa@unirc.it (F. Ruffa), mariacarla.lugara@unirc.it (M. Lugarà), gaetano.fulco@unirc.it (G. Fulco), filianoti@unirc.it (P. Filianoti).

https://doi.org/10.1016/j.measurement.2024.114246
Received 13 June 2023; Received in revised form 11 December 2023; Accepted 27 January 2024
Available online 3 February 2024

focus on the characterization of a submerged U-OWC system. It is a completely submerged device, consisting of a caisson with a vertical inlet duct and a pressurized air cushion in the upper part of a chamber. The natural oscillation frequency of the water column varies depending on the air pressure in the chamber. When this frequency approaches that of the waves, the system absorbs energy, causing a reduction in the wave motion. Electricity is then generated by a hydraulic turbine located in the vertical duct [19].

For characterizing the producibility of these types of plants, we need to evaluate the percentage of kinetic energy transported by the waves absorbed by the system, and therefore available for conversion. The hydrodynamic efficiency of an OWC system can be calculated as the ratio between the pneumatic power and the average energy flux of the incident waves. This is known as the Capture Ratio. In emerging plants, the pneumatic power available to the Power Take Off (PTO) is estimated. In submerged systems, since there is no exchange of air mass with the atmosphere, the estimation of performance must be done through a combined measurement of pressure and velocity in the duct or chamber.

Several Authors proposed different experimental setups to calculate the Capture Ratio, utilizing different techniques to determine the energy flux into the chamber. Each setup involves the use of various sensors to measure the required quantities. In emerged converters, the most commonly used devices are wave height meters [20], based on Doppler effect sensors [21], rotational systems [22], radar level sensor [23], pressure sensors [24]. While in the submerged devices, the most used sensors are the pressure transducers [13].

Specifically, in the case of U-OWC, the flow rates in different sections are linked to each other by the mass conservation law. By measuring the flow rate at the inlet duct, it is possible to calculate the water discharge into the chamber, necessary for the calculation of the system efficiency [25].

This implies the need to measure the speed, which can be done using direct or indirect speed measurement methods. For direct detection, rotational measurement systems are widely used and easy to operate. By counting the revolutions and angular velocity, these systems enable the determination of fluid velocity. In the case of U-OWC, this type of sensor can be installed in the vertical duct, where the flow velocity distribution is more homogeneous along a section than in the chamber, where there is a free surface. Anyway, the placement of an obstacle in the duct can introduce a disturbance in the flow, affecting both the accuracy and the plant performance. In addition, mechanical systems are more prone to wear and breakage and require periodic cleaning of the rotating parts from the marine vegetation. Another emerging measurement technique involves the use of Acoustic Doppler Current Profiler (ADCP) systems to detect the absolute speed of water. Their operating principle is based on Doppler effect, in particular the Doppler shift [26]. The problems related to their use is that they are often bulky and require batteries and an internal data logger. In addition, periodic interventions are necessary to prevent battery depletion and the growth of algae on the transducers [7].

The other possibility is to indirectly measure the speed of water, by measuring the instantaneous displacement of the water surface inside the chamber, and deriving it to obtain the velocity. Three types of sensors are commonly used for water level measurements: float meters, pressure sensors [27] and non-contact distance meters [27–29]. For applications on U-OWC systems, the main methods involve the use of pressure sensors or ultrasonic distance meters [17]. Water level detection with non-contact sensors has the advantage that the instrument is not directly exposed to water, making it more robust to erosion effects [30]. Ultrasonic devices operate by generating a pulse or series of pulses in the ultrasound range and measuring the time it takes for the device's receiver, often a piezoelectric transducer, to detect the pulses [30,31]. This solution has some critical aspects, since ultrasonic systems, to work properly, need to be installed at a precise angle (90°) respect to the surface to be detected, so as to receive the echoes reflected by the water surface. In presence of a sloped surface, such as inside the chamber of a U-OWC, there may be missing echoes that could compromise the accuracy of the measurements. Additionally, maintaining the sensors can be challenging as the housing site may not be easily accessible. Ultrasonic sensors require frequent monitoring as the formation of patinas or condensation could affect their proper functioning. In addition, to improve measurement accuracy, the variation in the speed of sound in air due to changes in temperature and density should be considered [32]. As previously mentioned, pressure sensors can be utilized in this type of application, as they offer a fast response time, high precision, and durability. By measuring the pressure at well-defined points using a pair of sensors, it is possible to calculate the acceleration and integrate velocity of the water [33]. Unfortunately, they are too bulky to be installed in the vertical duct of a small scale U-OWC [26].

Moreover, all the instrumentation mentioned above has to be waterproof and it is non-miniaturizable, so that it cannot be used in scale experiments, that are very common in this research area [34–39].

To overcome all the above cited difficulties, in [40] it is proposed an innovative indirect measurement system, based on the measurement of thermodynamic quantities of the air mass inside the plenum, such as pressure and temperature, using commonly used sensors, like pressure sensors and thermocouples. Compared to the methods described above, the proposed approach offers several advantages. Firstly, it does not interfere with the hydrodynamics of the system, thus minimizing any impact on the plant's performance. Secondly, it employs widely available, robust, and cost-effective sensors. Additionally, the sensors are positioned within the air chamber, allowing for improved durability since they are not in direct contact with seawater.

The method was applied to verify whether a strong natural resonance can be obtained by tuning the mass of air pocket inside the plant and checking the computational algorithm. No details were given concerning validation procedure of the proposed methodology. The present work aims at validating and upgrading the method above cited. To this aim, we reproduced numerically an experiment on a U-OWC rel.1 plant, having the same size of the physical one tested by [13,40], and subjected to the same waves having the same energy content as the sea waves.

Section 2 presents the method to estimate the plant performance and prescribes the 2D numerical simulations. Section 3 presents thew results of the numerical simulations and check the 1D mathematical model. Section 4 characterizes the thermal measurement system and carries out the correction necessary to overcome the insufficient time of response of the gauge. Section 5 summarizes the result of the work.

2. The wave-U-OWC interaction

2.1. Estimation of the captured energy

U-OWCs are wave energy converters characterized by the presence of a vertical conduit before the plenum chamber, which gives the device a typical U-duct shape. They are embodied in a concrete caisson, close to each other to form an upright (or submerged) breakwater. Each caisson contains several cells, separated from each other by dividing walls (see Figure 3 of [13]). The first mathematical description of the hydrodynamics inside a U-OWC device, both submerged and upright breakwater, was proposed in [13]. Afterwards, the flow motion inside the U-OWC was studied by [14–16,41]. Recently, a comparison between 2D CFD model and 1D model of the fluid dynamics inside a U-shaped OWC device was conducted by [42]. This phenomenon has been analyzed under the hypothesis of stream currents, in that the flow motion has a predominant direction.

A method to evaluate the energy flux captured by an U-OWC plant, was investigated through a field experiment on a 1:10 model [13,40]. This method is based on the measurements of the temperature and pressure fluctuation inside the plenum chamber. Following the procedure

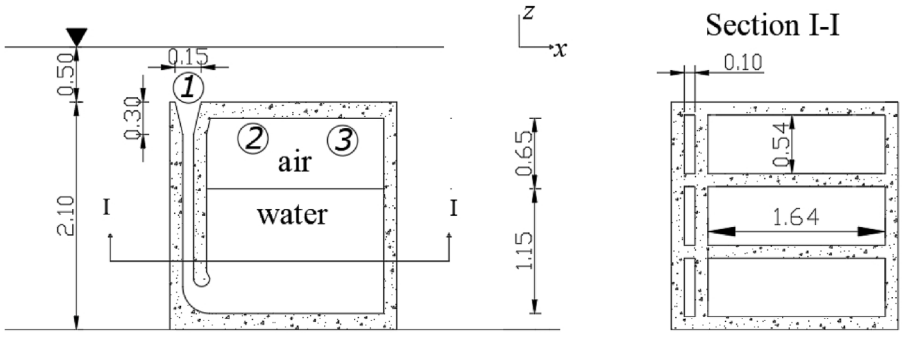

Fig. 1. Reference scheme for the positioning of the pressure transducers and the temperature gauge. The dimension of the plant are in meters and are the same described in [40].

described by [13,40], three measurement instruments are employed: transducer ① measures the water pressure at the upper opening of the vertical duct; transducer ②, the pressure in the plenum, transducer ③, the air temperature in the plenum (see Fig. 1).

Knowing the pressure inside the plenum, and considering that the air mass in the plenum is constant, the instantaneous volume of the air mass can be evaluated by means of the perfect gas law:

$$p_a V_a = M_a R T_a, \tag{1}$$

and consequently, the free surface displacement ξ, of the water interface in the plenum can be evaluated by means of

$$\xi = \frac{1}{A_c}\frac{\partial V_a}{\partial t}, \tag{2}$$

being A_c, the area of the horizontal section of the plenum chamber.

Finally, we obtain the velocity u_z, in the vertical duct which is related to the time derivative of the free surface displacement inside the chamber by means of the continuity equation:

$$u_z = \frac{s''}{s'}\frac{\mathrm{d}\xi}{\mathrm{d}t}, \tag{3}$$

where s' is the width of the vertical duct, and s'', the width of the oscillating water column in the chamber.

The energy flux per unit length, captured by the plant can be calculated as:

$$\overline{\Phi}_{abs} = \frac{1}{T}\int_0^T \Delta p(t) u_z(t) s' \mathrm{d}t, \tag{4}$$

being Δp the pressure fluctuations measured by transducer ① at the outer opening of the vertical duct.

2.2. The 2D numerical experiment

In order to evaluate the captured energy by the submerged U-OWC of Fig. 1, under the action of the waves, a CFD simulation has been carried out. Being each cell independent of the other (see Section I-I in Fig. 1), the simulation is carried out only on one cell forming the caisson breakwater. Moreover, we can effectively recur to a two-dimensional domain, due to the fact that the cell width is much smaller than its length. The computational domain is constituted by a wave-flume, with a piston-type wavemaker, placed at the left extremity, and a submerged breakwater embedding an U-OWC plant, in the middle. The position of the device was chosen to achieve stationary conditions in the nearby of the plant, for a time interval of several wave periods, avoiding the wave radiated from the submerged breakwater are reflected at the flume extremities. The 2D wave flume is 165 m long and 4.1 m high, as shown in Fig. 2. The U-OWC breakwater has the same size of the plant described in [40].

Some preliminary simulations were conducted in order to evaluate the eigenperiod of the plant, setting the mass of the air in order to achieve the resonance condition with the same waves having the same energy content as the sea waves occurred during the field experiment of [40]. In detail, we have evaluated the height of the air pocket, ξ_0 (measured from the ceiling of the caisson) and the time period to achieve the still water conditions. To evaluate the natural frequencies of the plant, some preliminary numerical tests have been carried out. These simulations consist in producing unforced oscillations in the U-duct (i.e. in calm water), assigning the initial position ξ_0, of the air–water interface in the chamber and the initial air pressure in the chamber, unbalanced with the external hydrostatic pressure. These initial conditions produce free oscillations around the equilibrium position. The eigen period of the plant is calculated averaging the periods of these oscillations. Table 1, shows the configuration simulated.

Table 1
Height at rest of the air mass, ξ_0 inside the chamber and the related eigenperiod.

ξ_0 [m]	T_e [s]
0.65	2.2

The spatial discretization of the computational domain was made by a hybrid mesh. *All Triangle Method* was used to discretize the overall length of the flume whilst, near the U-OWC device, rectangular elements were adopted (see Fig. 3). Air is compressible and, in the nearby of the structure, the $k-\omega$ turbulence model was set (for more information see [25,42,43]).

The wave generation process has been simulated assigning a sinusoidal motion to the left wall of the wave flume (see the wavemaker in Fig. 2), by means of a *User Defined Function* (UDF). The maximum displacement of the piston type wavemaker was evaluated as reported by [44], for the first order piston wavemaker solution.

The numerical 2D unsteady simulation is based on the Eulerian approach, using the commercial code Ansys Fluent v17.0, Academic Version. The water–air interaction is taken into account by means of the *volume of fluid* (VOF) model. In the VOF model, two or more fluids (or phases) are not interpenetrating, and the fraction of the volume of the qth phase in a cell is called the volume fraction, $\alpha_q \in (0,1)$. Each volume fraction is governed by its own continuity equation. The *geometric reconstruction* is the scheme used to evaluate the volume fraction in a cell hosting an interface between air and water, and the interface between this two fluids is calculated by a piecewise linear interpolation. Both fluids are assumed to be unsteady and are computed solving the governing equations (*i.e.* the mass conservation, or continuity, equation, the momentum balance equation and the energy conservation equation). In this work, the governing equations were discretized according to a finite volume approach, adopting an implicit formulation for the *pressure-based* algorithm.

The *Semi-Implicit Method for Pressure-Linked Equations Consistent* scheme (SIMPLE-Consistent) was used for the pressure–velocity coupling. This is a segregated algorithm that uses a relationship between velocity and pressure corrections to enforce mass conservation and to obtain the pressure field. In order to obtain the spatial discretization of

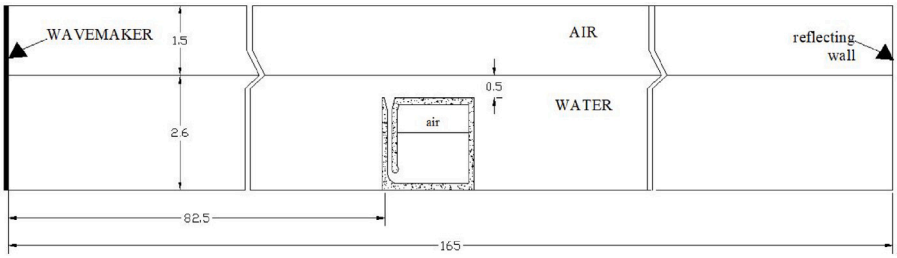

Fig. 2. Sketch of the computational domain and of the U-OWC breakwater.

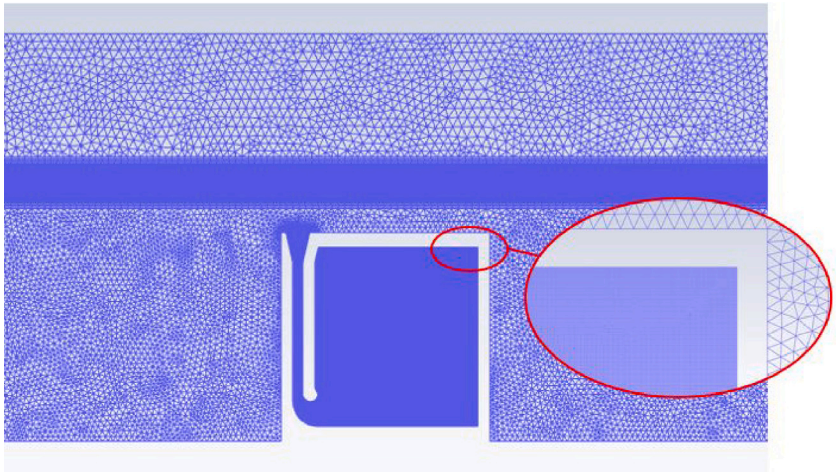

Fig. 3. Spatial discretization of the computational domain. See the refinement in the nearby of the U-OWC breakwater and of the free water surface.

Table 2
CFD simulation set up details.

Model for two-phase (water/air) interaction	*Eulerian VOF*
Solver	*SIMPLEC* algorithm
Spatial discretization of Gradient	*Green Gauss cell Based*
Spatial discretization of pressure	*PRESTO!*
Spatial discretization of momentum	*2nd order upwind*
Spatial discretization of density	*2nd order upwind*
Spatial discretization of Energy	*1st order upwind*
Spatial discretization of Volume Fraction	*Geo-Reconstruct scheme*
Transient formulation	*1st order implicit*
Energy AMG Method	*F-Cycle*
Time step	1/1000 [s]
Turbulence model	$k-\omega$ *- Standard*
Reference Pressure	p_0 = 101,300 [Pa]
Reference Temperature	T_0 = 299 [K]
Reference Density	ρ_0 = 1.225 [kg/m^3]

the convection terms in the governing equations, we used the Green-Gauss cell-based method for the gradient evaluation and the *PREssure STaggering Options* scheme (PRESTO!) for the pressure equation. The other convection–diffusion equations (e.g., momentum or energy equation) were discretized by means of the second-order upwind scheme. In order to keep the Courant–Friedrichs–Lewy number value much lower than 1 and improve the solution convergence, a time step $\Delta t = T/1000$ s was used. A summary of the CFD simulation set up details are shown in Table 2. For more details, concerning the CDF model, see [25,42,43].

3. Results of the experiment

3.1. Performance estimation

The mean energy flux Φ_{abs}, absorbed by the plant is evaluated by Eq. (4), integrating the product Δp by u, along the x-direction, at the upper opening of the vertical duct. Fig. 4 shows Δp and the pulsating discharge Q versus time. As said before, the best performance of the U-OWCs is achieved when the period of the incoming waves is equal to the eigenperiod of the plant [16]. In other words, the less the shift in phase between the pressure fluctuation and the pulsating discharge is, the more the plant absorbs. If the pulsating discharge (as in this case of Fig. 4), anticipates the pressure fluctuation, the wave period is greater than the eigenperiod and some air need to be pumped into the plant to increase T_e [16,25]. On the contrary if the pulsating discharge follows the pressure fluctuation, the wave period is smaller than the eigenperiod of the plant and some air need to be exhausted from the plant to reduce T_e.

The elemental flux along a horizontal section of the vertical duct was calculated numerically, by considering 3 points along the x-axis at an interval Δx = 0.03 m. The energy flux, was evaluated at z = 0.9 m, below the still water level, that is 0.4 m below the upper opening of the U-duct, in order to evaluate the captured energy flux, net of the minor losses occurring at the upper opening. Fig. 5 shows the energy flux absorbed by the plant.

The pulsating discharge through the U-duct produces an oscillation of the air–water interface inside the chamber. Under the action of a wave crest, the water enters the duct and moves up the free surface inside the chamber, compressing the air mass in the plenum. In this condition, the air temperature increases from the still temperature. Whilst, when a wave trough passes over the upper opening of the plant, the water exits the plant and the free water interface inside the chamber moves down, decompressing the air mass in the chamber. Consequently, the temperature of the air mass decreases below the still temperature.

Fig. 6 shows the position of the air–water interface, at four given time instants during a wave period.

The wave pressure fluctuations on the outer opening of the plant cause the oscillation of the air water interface inside the chamber. Fig. 6

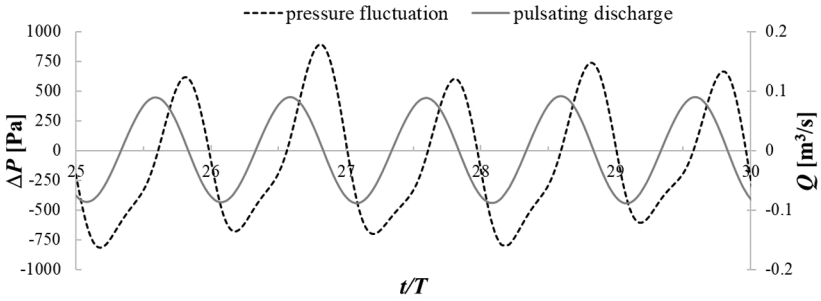

Fig. 4. Pressure fluctuation and pulsating discharge versus time.

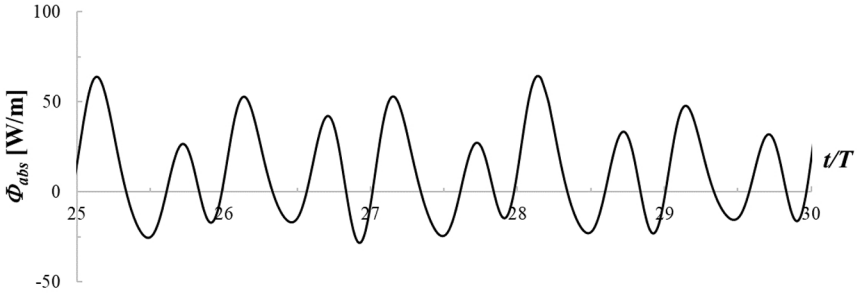

Fig. 5. Energy flux absorbed by the U-OWC plant ($H = 0.1$ m, $T = 2.2$ s).

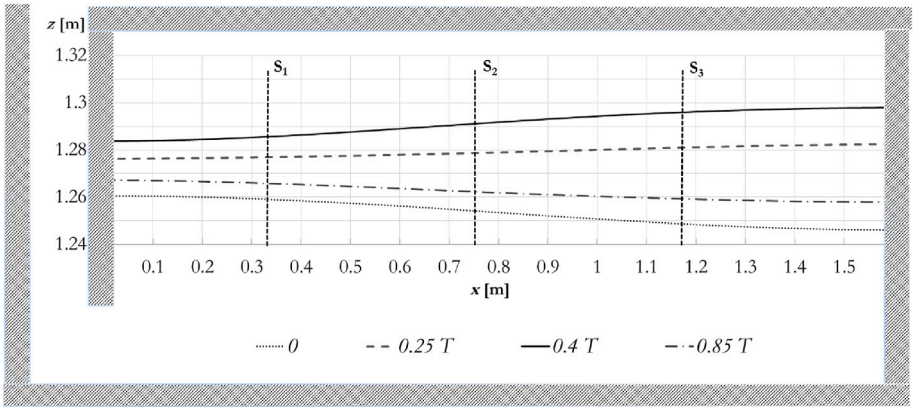

Fig. 6. Free surface elevation inside the chamber of the U-OWC.

shows the instantaneous position of the air water interface, at some given time instants. It is worth to note that the water level inside the plenum is not horizontal, whichever the time instant is. Furthermore, the amplitudes of oscillations around rest position, increase moving from the abscissa S1 to the abscissa S3. Fig. 7 shows the time history of the free surface displacement in the three abscissa of Fig. 6. As we can observe, the maximum vertical displacement occurs along the vertical wall in the lee side (the nearest to section S3), and it consists in over 4 cm.

Fig. 8 reports the time averaged value of the surface displacement in the sections S1, S2 and S3 compared to that at the section S2. As we can see they are quite similar, marking abscissa S2 the most representative of the average volume, where putting a level gauge.

To evaluate the variation of the air temperature inside the plenum, produced by the oscillation of the water surface, six points equally spaced in the air volume were considered (see Fig. 9).

As we can see, despite the asymmetrical variation of the volume of air inside the chamber, the fluctuation of the air temperature inside the plenum is space independent. The percentage difference between the dashed line (named T5) and the continuous gray line (named T3) is about 0.1%. This permits us to deduce that the position where to measure the temperature can be chosen arbitrarily. In the following, we will refer to the average value T_a of the air temperature. In Fig. 10, the average temperature and the pressure fluctuation inside the air chamber, are shown.

Table 3
Summary of the results of CFD simulations.

H [m]	T [s]	ξ_0 [m]	ΔT_a [K]	$\overline{\Phi}_{abs}$ [W/m]
0.1	2.2	0.65	6.9	11.21

Table 3 shows a summary of the results of the CFD simulations for the wave train simulated.

3.2. Check of the 1D mathematical model

The performance in the field of a physical plant can be evaluated through a 1D mathematical model, using as input the measurements of the pressure fluctuation at the upper opening of the plant, the air pressure and the temperature fluctuations inside the plenum chamber, following the procedure described in Section 2.1. In order to check

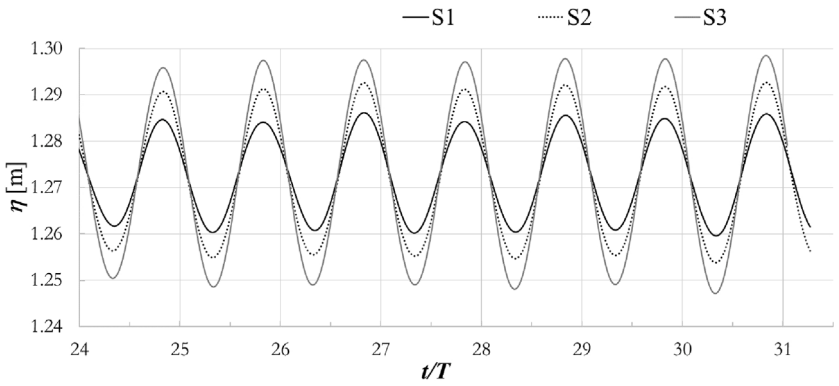

Fig. 7. Free surface displacement around the rest position inside the chamber at sections S1, S2, ans S3, as indicated in Fig. 6.

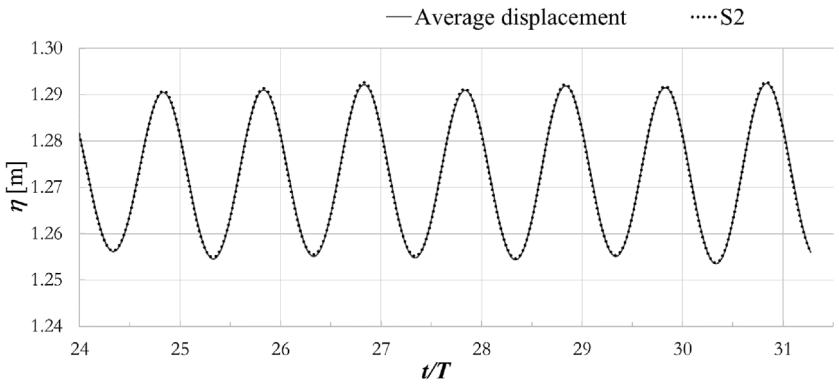

Fig. 8. Comparison between the free surface elevation inside the chamber of the U-OWC at abscissa S2 and the average free surface displacement.

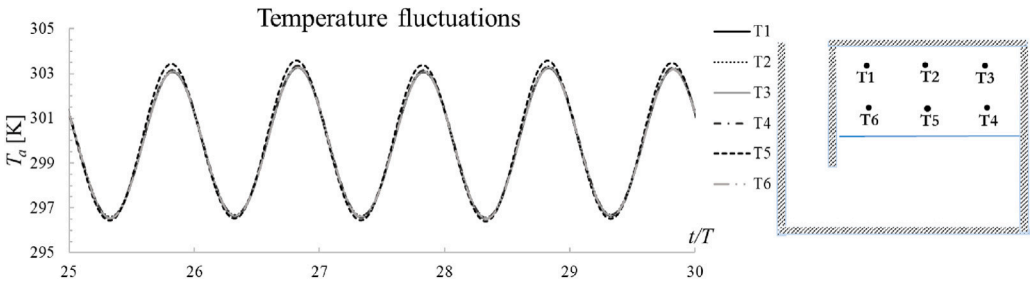

Fig. 9. Fluctuations of the air temperature inside the plenum chamber vs. time.

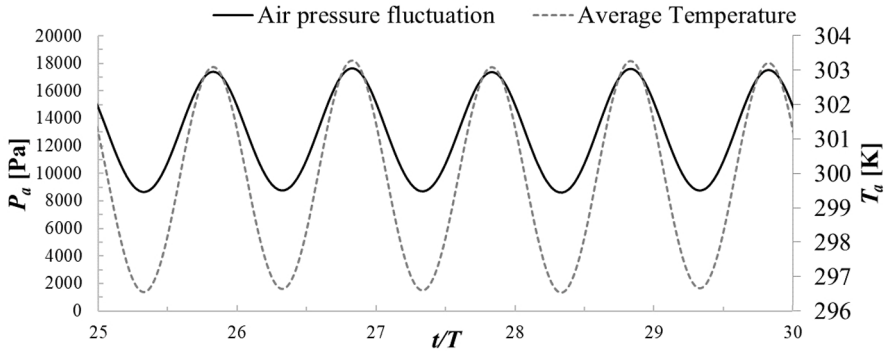

Fig. 10. Fluctuations of the air pressure and of the average air temperature inside the plenum chamber.

the 1D mathematical model, we used the results of CFD simulations as input and compared the output of the 1D and 2D models. Specifically, we utilized the pressure fluctuations at the upper opening and the air temperature fluctuations inside the chamber obtained from the 2D simulations as input for the 1D model. The variation of the air volume in the plenum, and consequently ξ, were evaluated by means of the

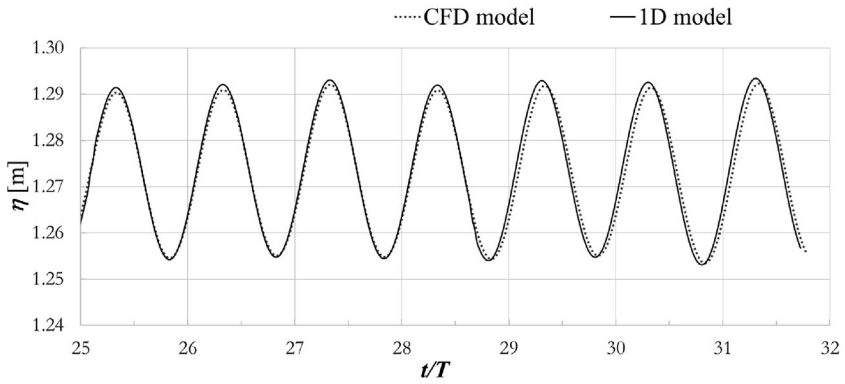

Fig. 11. Time history of the free surface elevation inside the chamber of the U-OWC: continuous line was obtained by means of the 1D model; dotted line, by CFD model.

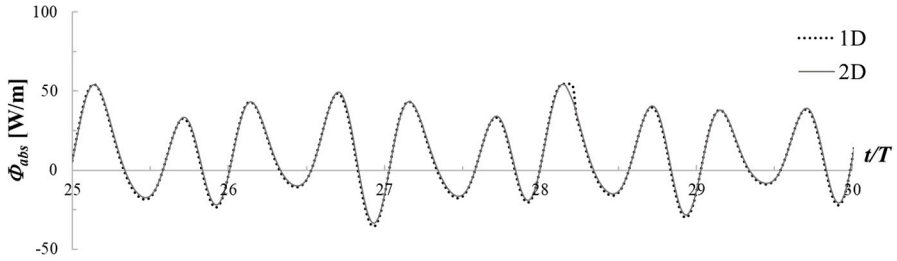

Fig. 12. Energy flux absorbed by the plant U-OWC breakwater: dotted black line was obtained starting from the temperature inside the chamber by means of the 1D model; continuous gray line was obtained by 2D simulation (the same of Fig. 5).

state law Eq. (1) and Eq. (2). Fig. 11 shows the oscillation of the free surface displacement inside the chamber versus time. In detail, continuous line represents the free surface elevation, evaluated starting from the temperature inside the chamber by means of the 1D model. Whilst, the dotted line represents the mean free surface displacement, obtained by the CFD simulations shown in Fig. 8.

As we can see, there is a very good agreement between the two curves. As a consequence, we have an accurate estimation of the water discharge in the plenum and then in the U-duct. By integrating the product of water discharge by the pressure fluctuation (see Eq. (4)), the energy flux absorbed by the plant has been evaluated, as shown in Fig. 12. It is possible to notice that, the two curves, the dotted black line, obtained starting from the temperature inside the chamber by means of the 1D model, and the continuous gray line, obtained by 2D model, are quite coincident.

3.3. Thermodynamic analysis

Assuming that the air mass transformation inside the plenum can be represented with a polytropic law, we have:

$$PV^{\gamma} = \text{const}, \tag{5}$$

being γ, the exponent of the polytropic transformation. Making explicit the volume V in Eq. (5), and substituting it in the perfect gas law (Eq. (1)), we have:

$$P_a \left(\frac{M_a R T_a}{p_a} \right)^{\gamma} = \text{const}, \tag{6}$$

that can be rewritten as:

$$T_{a0} P_{a0}^{\left(\frac{1-\gamma}{\gamma}\right)} = T_a P_a^{\left(\frac{1-\gamma}{\gamma}\right)}, \tag{7}$$

being T_{a0} and P_{a0}, the initial value of the temperature and the pressure of the air inside the plenum chamber, respectively. Varying the value of γ, from the isothermal ($\gamma = 1$) to the adiabatic ($\gamma = 1.4$) transformation, the fluctuation of the air temperature can be evaluated.

Fig. 13 shows the comparison between the temperature fluctuation for different values of γ and the actual temperature, evaluated as reported in Section 3.1. To be more precise, the figure displays five curves labeled as T1, T1.1, T1.2, T1.3, and T1.4, where each number corresponds to the exponent value of the polytropic law. The actual temperature, previously shown in Fig. 9, is also indicated.

As we can see, the actual temperature fluctuation, in dashed red line, perfectly matches the adiabatic curve ($\gamma = 1.4$), represented in continuous black line. This result agrees with the setting of the CFD simulation, in which no heat wall exchange has been considered.

The captured energy fluxes for the values of γ, previously indicated, are shown in Fig. 14. The maximum energy captured by the plant occurs in the case of isothermal transformation (see continuous gray line, name T1). Indeed, during an isothermal transformation, the cyclic work done during compression–expansion is larger than in the other transformations for the same pressure fluctuation.

Table 4 shows a summary of the results of the sensitivity analysis on the exponent of the polytropic transformation. In detail, it shows how the captured energy changes, on varying the amplitude of oscillation of the air temperature. To specify, considering $\gamma = 1$ (*i.e.* isothermal transformation), the temperature inside the plenum is constant, and equal to the initial air temperature (about 300 K), and the percentage variation of the air volume reaches its maximum; as a consequence the energy captured by the plant, depending linearly by the discharge (see Eq. (4)), reaches its maximum. On the contrary, considering $\gamma = 1.4$ (*i.e.* adiabatic transformation), the amplitude of the temperature fluctuation is seven Kelvin, the percentage variation of the air volume reaches its minimum, and consequently the energy captured by the plant is minimum too, and it has same value as obtained by means of the CFD simulation.

To summarize, the energy captured by the plant decreases as γ increases, because of the reduction of the amplitude of the fluctuation of the air volume inside the plenum.

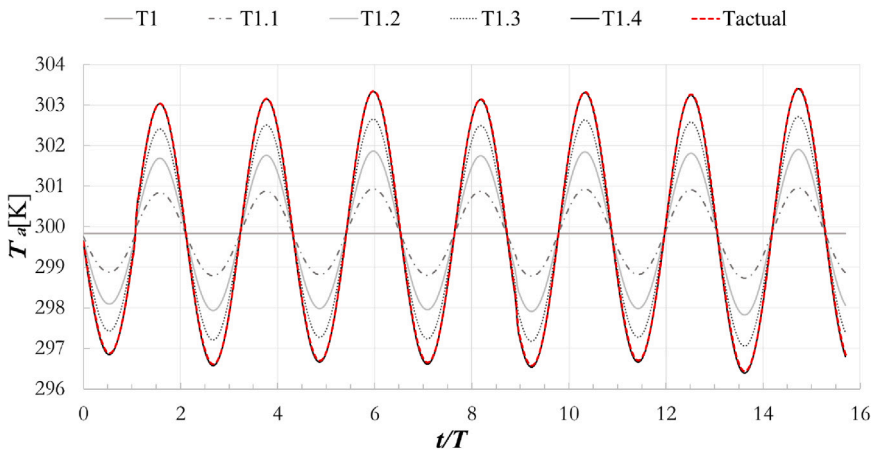

Fig. 13. Temperature fluctuation inside the plenum evaluated by means of Eq. (7), varying the value of γ.

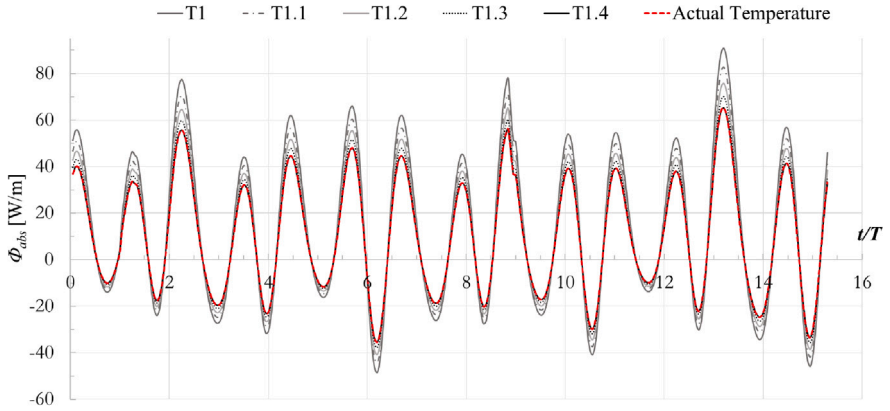

Fig. 14. Captured energy flux evaluated by considering the temperature fluctuations shown in Fig. 13.

Table 4
Summary of the results of the sensitivity analysis.

γ [-]	ΔT_a [K]	$\Delta V_a/V_0$[%]	$\overline{\Phi}_{abs}$ [W/m]
1	0	8.9	13.9
1.1	2.2	8.1	12.7
1.2	4.1	7.5	11.7
1.3	5.6	6.9	10.8
1.4	7.0	6.4	10.3

4. Characterization of the thermal measurement system

4.1. Determination of time response requirements

In order to obtain indirect flow measurement in OWC systems, through the measurements of the air temperature in the air chamber, we need a fast enough temperature sensor to follow the rapid temperature variations, due to compression and decompression of the air in the plenum. Considering as input to a real gauge the actual fluctuations T_{act}, of the temperature of the air in the plenum (i.e. the temperature measured by an ideal gauge) shown in Fig. 10, the measured temperature T_{meas}, will be affected by the dynamic behavior of the gauge, both in terms of amplitude and phase angle. A thermocouple (TC) behaves as a typical first-order dynamic system due to its heat transfer properties. This approximation is quite common, in the hypothesis of working in the linear range of the thermocouple and assuming that there are no changes in the operating conditions during the measurements [45–48]. Due to the close connection between the dynamic properties of a thermocouple and its operating conditions, it is essential that the calibration environment closely matches or resembles the actual application environment. In these hypotheses, assuming that the sensor can be mathematically represented by a first order instrument, we have:

$$a_1 \frac{dT_{meas}}{dt} + a_0 T_{meas}(t) = b_0 T_{act}(t), \tag{8}$$

that can be rewritten as:

$$\frac{a_1}{a_0} \frac{dT_{meas}}{dt} + T_{meas}(t) = \frac{b_0}{a_0} T_{act}(t), \tag{9}$$

and by defining:

$$\tau \equiv \frac{a_1}{a_0}, \tag{10}$$

$$K \equiv \frac{b_0}{a_0}, \tag{11}$$

we arrive to

$$\tau \frac{dT_{meas}}{dt} + T_{meas}(t) = K T_{act}(t). \tag{12}$$

Term K is the static sensitivity of the system, and represents the amount of output per unit input when the input is static; it has the dimension of the output divided by the input; τ is the time constant of the system and is experimentally determined as the time needed by the output to achieve 63.3% of its final value, after a step change in the input [49–51]. To find 'τ' and assess the instrument's dynamic performance, it would be necessary to apply sinusoidal-type temperature inputs, but it is difficult to generate this type of signal, so standard types are used, such as the step signal. There are three principal methods to determine 'τ' [52–57]:

Table 5
Relative error between standard deviations of the actual temperature fluctuations and measured ones, through a first order instrument, having different values of τ.

$\tau[s]$	e_τ [%]
0.01	0
0.05	0.3
0.1	0.9
0.2	3.2
0.3	6.7
0.4	11
0.5	15.7
1	37.5
2	59.8
4.5	70.9

- Look for the moment when the output signal reaches 63.3% of the final value after the step. This method is simple but less accurate due to the uncertainty in the step application time.
- Draw a tangent at the start of the temperature change caused by the step, intersecting it with the final value. The x-axis intersection point gives 'τ'. This method is more accurate but still sensitive to initial curve errors.
- Use a logarithmic scale to perform linear regression on data points derived from the sensor's response. The slope of the resulting line provides 'τ'. This method offers good accuracy and is suitable for first-order instruments.

Introducing the operational transfer function of the system:

$$\frac{T_{meas}(t)}{T_{act}(t)}(D) = \frac{K}{\tau D + 1}, \tag{13}$$

where D is the differential operator, we can obtain the response to any given input, by solving the differential equation. We need to evaluate how the time response of the temperature gauge affects the evaluation of the plant performance. To this aim, we simulated the response of a real gauge represented by Eq. (13), for different values of τ, fixing $K = 1$ and applying as input $T_{act}(t)$, the temperature fluctuations obtained through the CFD simulation (i.e. the curve represented in Fig. 9).

The results obtained solving Eq. (13) are summarized in Table 5, in terms of relative error between the standard deviations of the input (T_{act}) and the output signal (T_{meas}), for different values of τ:

$$e_\tau = \frac{|\sigma_{T_{act}} - \sigma_{T_{meas}}|}{\sigma_{T_{act}}}. \tag{14}$$

The graphical results for $\tau = 0.05s$, $0.5s$ and $4.5s$ are showed in Fig. 15.

As it can be seen, if $\tau \leq 0.1s$, the sensor can faithfully reproduce the temperature variations in time, with more than 99% of accuracy. Increasing τ, the sensor performances worsen, losing completely the capacity to follow the temperature fluctuations, as τ approaches the period of oscillation of the air temperature (see Fig. 15(c)). In the following Section, we evaluate how an error in the temperature measurement affects the measurement of captured power by the OWC system.

4.2. Influence of the sensor response in evaluation of the power captured by the plant

Fig. 16 shows the comparison between the actual temperature T_{act}, evaluated by means of the CFD simulation, and the temperature T_{meas}, measured by a sensor with a first order response, as described in the previous Section, considering several values of τ up to 0.5s.

As the reader can see, as the time constant τ increases, the amplitude of the temperature fluctuations become smaller and the time shift, larger. For $\tau = 0.5s$, the amplitude of T_{meas} is halved compared to the actual one, T_{act}. The phase shift passes from zero, for $\tau = 0.01s$ to 109 degree, for $\tau = 0.5s$.

Table 6
Summary of the simulation for different values of τ.

τ	T_{max}	T_{min}	ϵ	$\overline{\Phi}_{abs}$	e_Φ	e_τ
[s]	[K]	[K]	[rad]	[kW/m]	[%]	[%]
0.01	303.4	296.4	0	8.2	21	0
0.05	303.4	296.5	0.31	7.1	32	0.3
0.1	302.9	296.9	1.26	5.6	46	0.9
0.3	302.5	297.2	1.57	6.1	41	6.7
0.5	301.9	297.9	1.9	7.9	23	15.7
1.0	301.0	298.7	2.8	10.9	6	37.5

Following the procedure described in Section 2.1, considering as input the temperatures shown in Fig. 16, we calculated the energy flux captured by the plant, which is shown in Fig. 17. For comparison, the energy flux obtained by means of the CFD simulation is also shown.

In Table 6, a summary of the simulation results are reported. The error e_Φ, in estimation of the energy flux Φ_{abs}, captured by the plant is due to the error on temperature measurements e_τ. As we can see, the error e_Φ, gets larger at the increasing of τ, reaching the maximum value of 46% for $\tau = 0.1$ s, while the energy flux $\overline{\Phi}_{abs}$ becomes progressively smaller. As τ increases from 0.1 to 1.0, the error becomes progressively smaller, and the energy flux grows, the more the larger τ is. The amplitudes of temperature fluctuations (i.e. $\Delta T = T_{max} - T_{min}$) shrink the more τ becomes larger, the opposite happen to the phase shifts ϵ, who become larger. The shrinking of ΔT and the increasing of ϵ produce an opposite trend on the estimation of the energy flux. Specifically, a reduction in the amplitude of the temperature fluctuation leads to an increase in the energy flux captured by the plant, as explained in detail in Section 3.3. On the contrary, the increasing of the shift of the phase angle brings to a reduction of the energy flux. For τ larger than 0.1, the shrinking of the amplitude of the temperature fluctuations play the predominant role.

4.3. Measurement optimization: an amplitude and phase correction technique

The temperature oscillations inside the plenum chamber are a result of the compression and decompression of the air caused by changes in the water level. This process is driven by the waves, and therefore, it shares the same period as the waves interacting with the plant. Knowing the frequencies associated to wind generated waves, the key issue in the design of the measurement system consists in choosing a sensor that has a cutoff frequency much greater than the maximum frequency in the bandwidth of wind generated waves (to stay safe we suggest a decade above). Several thermocouples can guarantee this requirement in their technical specifications, but the declared value consists in the intrinsic response time measured, according to IEC 60584–2013, into a medium with a high thermal capacity. The performance requirements in terms of time response apply to the entire measurement system in the specific operating conditions. Since the heat exchange between the ambient and the junction of the thermocouple is slower in air than in contact with liquid or solid materials, the actual time constant of the measurement system will be much higher than that declared in the sensor datasheet. Expressing the cutoff frequency as:

$$\omega_t = \frac{2\pi}{\tau}, \tag{15}$$

it is obvious that the faster is the measurement system, the more the cutoff frequency will be far from the operating frequency.

To increase the speed of the system, the only feasible approach is to enhance the heat exchange between the air and the sensor. This can be achieved by reducing the thickness of the junction and improving heat transfer through increased convection. However, it is important to note that these modifications would lead to substantial cost increases and

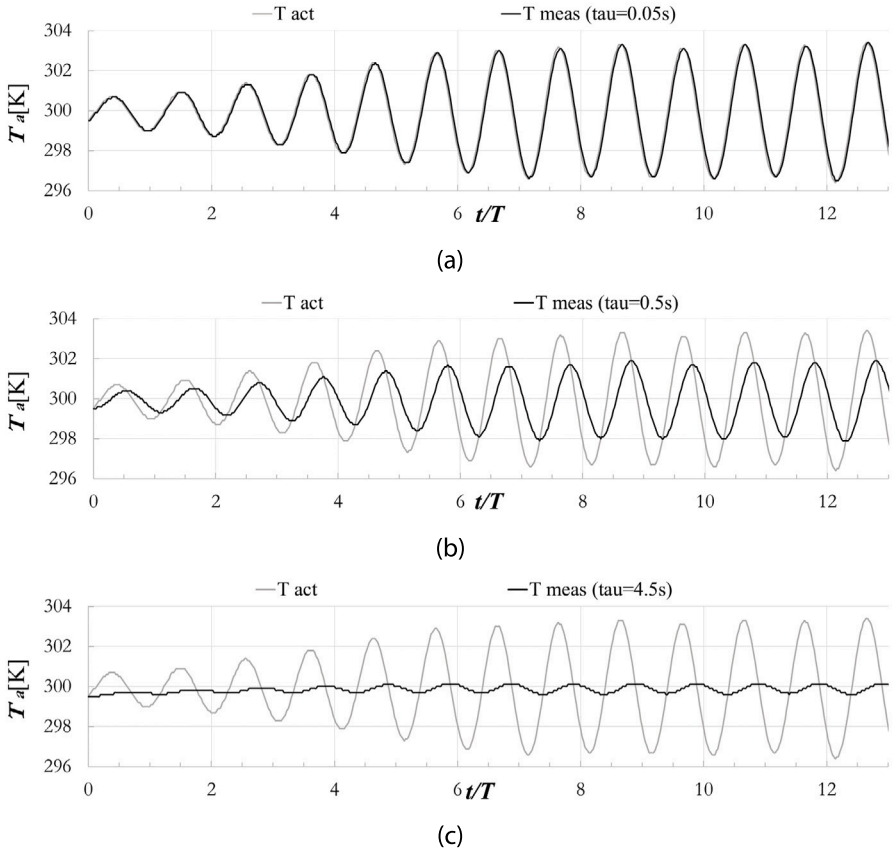

Fig. 15. Simulation of a first order response — temperature trend a) $\tau = 0.05s$, (b) $\tau = 0.5s$, (c) $\tau = 4.5s$.

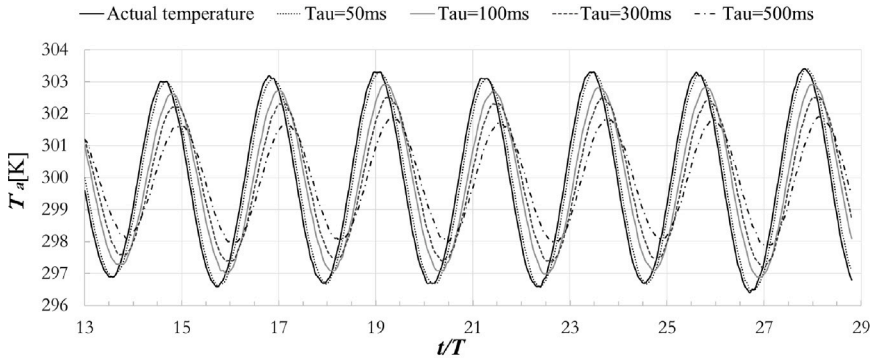

Fig. 16. Time history of the temperature inside the chamber. Continuous line represents the actual temperature, the other lines represent the temperature evaluated by means of Eq. (8).

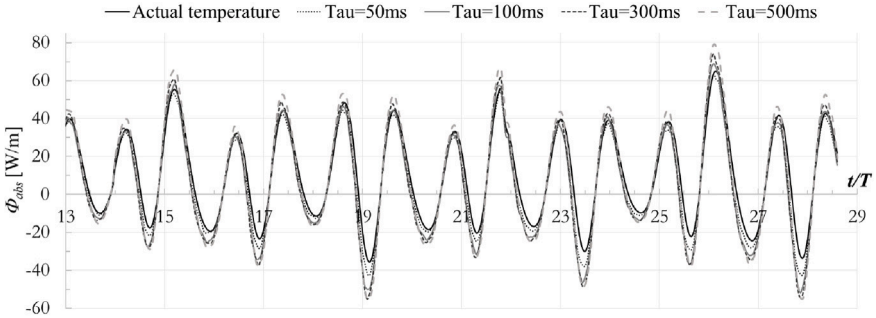

Fig. 17. Energy flux captured by the U-OWC plant: comparison between 2D model (actual temperature) and the results of the 1D model, obtained using as input the different temperature histories shown in Fig. 16.

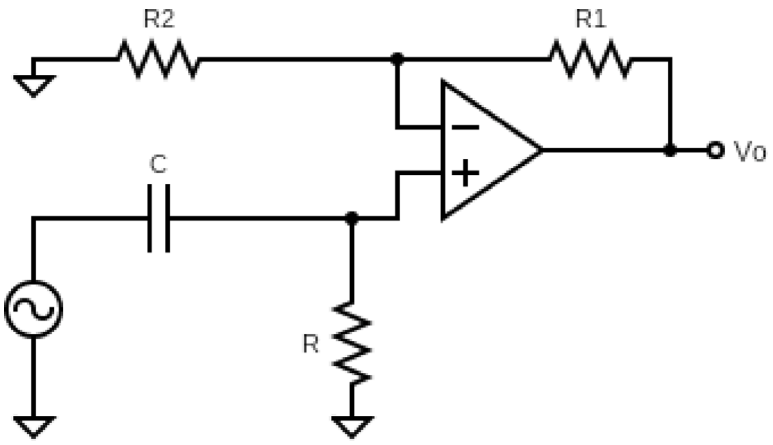

Fig. 18. Circuit diagram of an active high-pass filter.

a reduction in overall system robustness. Additionally, it is important to consider that there is a lower limit for the junction thickness that cannot be exceeded with the technologies currently involved, typically around 0.25 mm.

An alternative approach that can be considered is implementing a control system to correct for measurement errors. This control system would aim to compensate for any inaccuracies or deviations in the measurements, providing a means to improve the overall accuracy and reliability of the system. Since the measurement system has been modeled with a first order dynamics, as seen in Section 4.1, assuming that we can accurately know the cutoff frequency, we can project a control, which compensates for amplitude loss and phase shift and moves the "overall" cutoff frequency higher.

A dynamic system of any order can be represented through its Laplace transform:

$$F(s) = \mathcal{L}\{f(t)\} = \int_0^\infty f(t)\exp^{-st}\,\mathrm{d}t. \tag{16}$$

This lets to represent dynamic systems through algebraic equations in s-domain:

$$s = \sigma + j\omega \tag{17}$$

where s is a frequency parameter expressed as a complex number. So, it is possible to determine the output of a dynamic system to a given input, by solving the problem in the Laplace domain:

$$Y(s) = G(s)X(s), \tag{18}$$

where $X(s)$ is a generic input and $G(s)$ is the transfer function of the dynamic system:

$$G(s) = \frac{\prod_{i=1}^{m}(s - z_i)}{\prod_{i=1}^{n}(s - p_i)} = K\frac{\prod_{i=1}^{m}(1 + sT_i)}{\prod_{i=1}^{n}(1 + s\tau_i)}, \tag{19}$$

where the numerator of Eq. (19) is the product of the m zeros of the system, and the denominator is the product of the n poles of the system.

To go back to the time domain we perform an inverse Laplace transform:

$$f(t) = \mathcal{L}^{-1}\{F(s)\} = \frac{1}{2\pi j}\lim_{T\to\infty}\int_{\zeta - jT}^{\zeta + jT}\exp^{st}F(s)\mathrm{d}s. \tag{20}$$

where ζ is a real number.

The frequency response of the dynamic system described by the transfer function in Eq. (19) can be effectively visualized using Bode plots, which provide graphical representations of the magnitude and phase characteristics as a function of frequency. If we calculate the cutoff frequencies ω_z and ω_p as in Eq. (15), for zeros and poles, we have that each pole causes an attenuation in magnitude after the cutoff frequency with a slope of $-20dB/dec$ and a phase displacement which starts a decade before ω_p and finishes a decade after, reaching a phase displacement of $-90°$. Zeros on the other hand cause an increase in magnitude, after the cutoff frequency, with a slope of $+20dB/dec$ and a phase shift of 90°, starting a decade before and finishing a decade after the cutoff frequency.

The temperature sensor, whose mathematical model can be expressed by Eq. (12), with a given time constant τ, and $K = 1$, can be represented in the Laplace domain as:

$$T_{act}(s) - \tau_{tg}sT_{meas}(s) - T_{meas}(s) = 0, \tag{21}$$

where τ_{tg} is the time constant of the temperature gauge, with a transfer function $G(s)$ defined as:

$$T_{meas}(s) = G(s)T_{act}(s) = \frac{1}{1 + s\tau_{tg}}T_{act}(s) \rightarrow G(s) = \frac{1}{1 + s\tau_{tg}}. \tag{22}$$

The Bode plots for magnitude and phase for a temperature gauge operating in air with an actual $\tau_{tg} = 4.7s$, are shown in Fig. 19(a). As said, to extend the frequency response of the system, we need to design a control $C(s)$ capable to shift the cutoff frequency of the system towards higher frequencies. The simplest and most effective solution is to implement a zero-pole cancellation technique. Anyhow, this implies to design a control $C(s)$, with a single zero falling in a certain band, around the pole of the system. This means that $C(s)$ would be intrinsically unstable, and for this reason this solution has been discarded. A $C(s)$ incorporating a zero-pole pair is imperative to ensure both an expanded frequency response and system stability. While the most apparent solution would involve zero-pole cancellation, wherein a zero coincides with the system's pole and a pole is located at the new cutoff frequency, an alternative approach was chosen. This alternative centers on a control with a defined gain, a zero at the origin, and a pole placed at the new cutoff frequency. Such a control effectively takes the form of an active high-pass filter, which can be seamlessly realized both digitally and as an analog circuit downstream of the thermocouple. The circuit configuration is illustrated in Fig. 18.

The transfer function $C(s)$ of the filter in Fig. 18 can be written as:

$$C(s) = K_c\frac{s\tau_c}{1 + s\tau_c}, \tag{23}$$

where $K_c = 1 + \frac{R2}{R1}$ is the gain of the control and $\tau_c = RC$ its time constant. The system operates in an open-loop configuration. Considering that we know with a high level of confidence the value of τ_{tg} of the thermocouple, we can project a control using Eq. (23) and plot the Bode diagrams to compensate for losses caused by the thermocouple. To accomplish this, a careful selection of K_c and τ_c is essential. Considering the fact that a zero at the origin leads to a magnitude increase with a slope of +20 dB/dec, it becomes imperative to choose K_c and τ_c in such a way that the filter exhibits unity gain precisely at the thermocouple's cutoff frequency. This approach ensures that beyond this frequency,

the filter effectively compensates for the thermocouple's characteristics up to the new cutoff frequency. The strategy employed in this study involves designing a control featuring a gain of 40 dB, a zero at the origin, and a pole positioned two decades beyond the thermocouple's cutoff frequency:

$$C(s) = 100\frac{s * 0.01\tau_{tg}}{1 + s * 0.01\tau_{tg}}. \tag{24}$$

Considering the situation of Fig. 19(a), the Bode diagrams of the proposed control, for magnitude and phase, are shown in Fig. 19(b), while those of the entire input–output chain, once applied the correction are shown in Fig. 19(c).

As it can be seen in Fig. 19(c), there is a band between 0.2 Hz and 2 Hz where the control is capable of compensating the information loss and to faithfully reproduce the input signal in output. Instead, for frequencies lower than 0.2 Hz, the control implemented worsens the response performances of the system. This means that the control filters out the continuous component of the input, so we will see in output just the oscillatory component. To overcome this issue, the final value of the temperature is obtained by summing the output of the filter and the value of the temperature measured by the thermocouple.

To test the correct functioning of the proposed control, we performed some simulations of the open loop system described by

$$T_c(s) = C(s)T_{meas}(s) \tag{25}$$

where $T_c(s)$ is the output of the open loop implemented and $G(s)$ and $C(s)$ are described by Eqs. (22) and (24) respectively, with $\tau_{tg} = 4.7s$. The final temperature is obtained as

$$T_{out}(t) = T_{meas}(t) + T_c(t), \tag{26}$$

where:

$$T_{meas}(t) = \mathcal{L}^{-1}\{T_{meas}(s)\}, \tag{27}$$

$$T_c(t) = \mathcal{L}^{-1}\{T_c(s)\}. \tag{28}$$

Some preliminary tests on the correction method have been carried out, using sinusoidal inputs having frequencies distributed in the bandwidth of the correction filter. The results are summarized in Table 7 in terms of relative error, both applying the correction and not. The filter reduces the error below 4% for input frequencies up to 1 Hz. The relative error rises up to 14% when the input frequency reaches 2 Hz. Without any correction, the relative error is much higher, being more than 80%. The considered range of frequencies is very high in comparison to the frequencies of sea waves which represent the target of any conversion system. In general, the peak frequency of the spectrum of wind waves is larger than 0.2 Hz, for a full scale plant, and it is larger than 0.5 Hz, for the small scale plant investigated by [13,40]. Although the filter introduces a phase shift, which, as seen in Section 4.2, has a non-negligible impact on the error in the measurement of the energy flux, it is apparent from the Bode diagrams in Fig. 19 that within the relevant frequency range this phase shift's magnitude remains smaller compared to what it would be if the filter were not employed. This leads to a twofold advantage.

The effectiveness of the correction method is tested also using as benchmark the results of the numerical experiment illustrated in Section 3. To this aim, Fig. 20 shows the comparison between the actual temperature T_{act} (i.e. the temperature measured by an ideal gauge), and the temperature T_{meas}, measured by a first order gauge having $\tau = 4.5$ s, both without correction (the continuous black curve) and with it (dashed red curve). The damping in the temperature amplitude is more than 90%, and the shift in phase angle is about 90°. The power captured by the plant is very close to the value obtained if the transformation of the air mass would be isothermal, and therefore the error on the estimation is about 35%. T_{out} shows the temperature after the correction (red dashed curve). It fits perfectly the actual one.

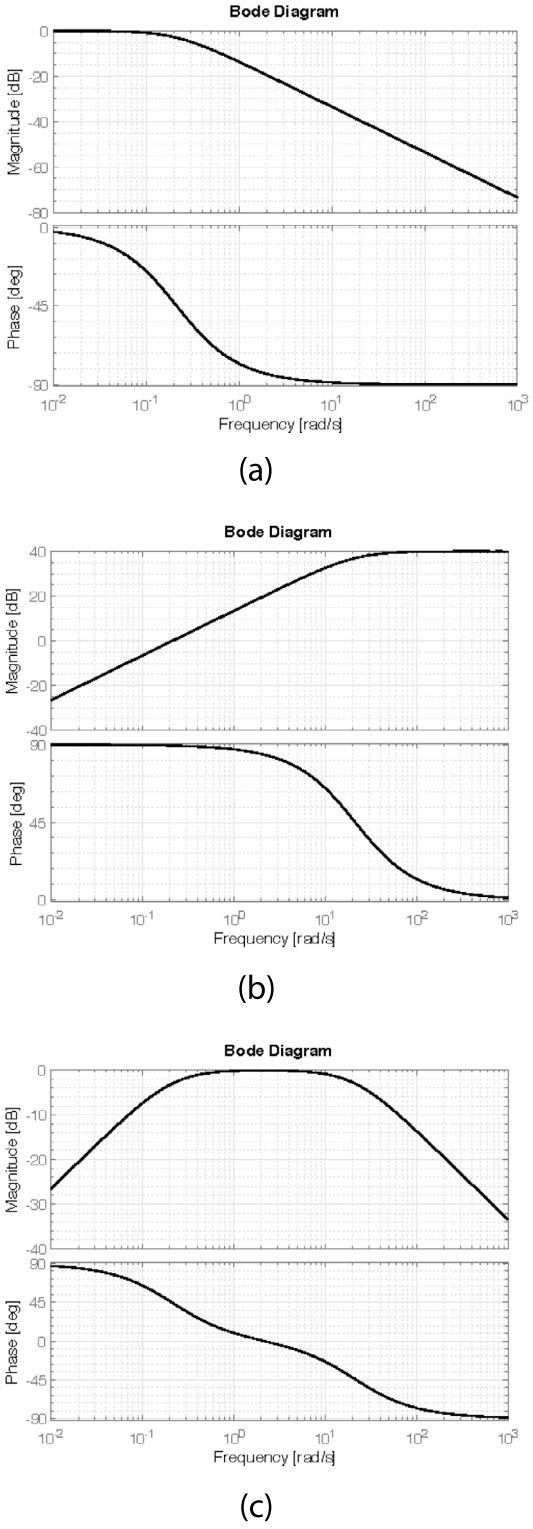

Fig. 19. Bode Diagrams of: the first order system representing a thermocouple with $\tau_{tg} = 4.7s$, the projected control, and the entire input–output chain: (a) Magnitude and Phase Plot for the thermocouple, (b) Magnitude and Phase Plot for the projected control, (c) Magnitude and Phase Plot for the output applying the control.

5. Conclusions

The measurement of the power captured by an energy conversion system is crucial to assess the performance of the converter. For a

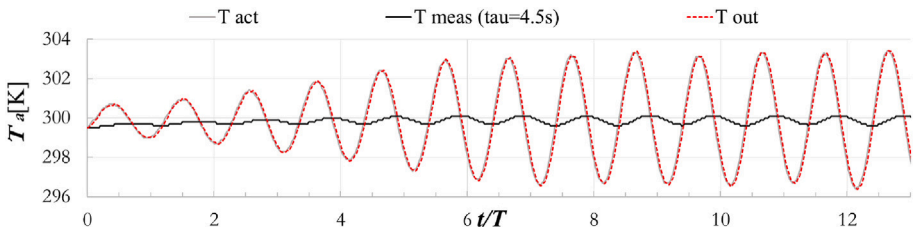

Fig. 20. Temperature fluctuations of the air mass inside the plenum of the U-OWC plant. The actual temperature T_{act}, is obtained through CFD simulation (see Fig. 9). T_{meas} is the temperature measured by a thermocouple, and T_{out} is the corrected temperature.

Table 7
Comparison of standard deviation of the input signal and output signal with and without correction, applying a 6 K peak to peak sine wave at different frequencies.

Signal frequency [Hz]	e_τ[%] without correction	e_τ[%] with correction
0.2	83.4	0.8
0.5	93.2	0.5
1	96.6	3.8
2	98.4	14

wave energy converter belonging to the U-OWC family, it requires to measure the water discharge through the plant. A non-conventional method was proposed by [13,40], substituting the measurement of the water velocity in the U-duct with the measurement of the air temperature fluctuations in the plenum. In this work, we have analyzed the influence of the installing point and of the time response of a thermocouple in the measurement of the energy flux captured by the plant. To this aim, we have reproduced a numerical experiment on the submerged U-OWC described in [40], in order to fully reproduce the dynamic behaviors of the conversion system.

Concerning the positioning of the temperature sensor, the CFD simulations have shown no spatial variation of the temperature inside the plenum, making irrelevant the position of the sensor inside the air mass. On the contrary, the water velocity varies significantly along the cross sections of both branches of the U-duct, making necessary multiple simultaneous measurements of the velocity in order to estimate the water discharge.

The time response of the temperature sensor greatly affects the measurement of the power captured by the plant, as demonstrated by a sensitivity analysis carried out simulating different types of air mass transformation (e.g. from isothermal to adiabatic). Results show that the energy flux is as higher as the amplitude of the air temperature fluctuation is small. Indeed, considering an isothermal transformation, with the temperature constant and equal to the initial temperature of the air in the chamber, the energy captured by the plant has its maximum. Supposing that the temperature sensor behave like a first order instrument, we have evaluated the captured energy fluxes, on varying the time response. The error in estimating of the energy flux was analyzed both in terms of damping in the amplitude and shift of the phase angle. In detail, the reduction of the amplitude of the measured temperature fluctuation produce an overestimate of the energy flux whereas, the forward shift of the phase angle brings to an underestimate of the energy flux.

Finally, we have proposed a methodology to correct the measurements of the temperature, by designing a proper high pass active filter. It operates introducing an appropriate gain in the frequency bandwidth, where the temperature signal is attenuated, because of the large response time. The filter was tested for particularly demanding conditions: response time up to 4.5 s and sinusoidal input up to 2 Hz. The filter worked well in all tests, exhibiting excellent agreement with the actual temperature obtained by means of the CFD simulation, and eliminating an error of about 38%, in the measurement of the captured power, which would be the same as the transformation be isothermal.

6. Symbols

Roman letters

A_c	[m^2]	Area of the horizontal section of the plenum chamber
a_0	[N/S]	Constant
a_1	[N/S]	Constant
b_0	[N/S]	Constant
CFD	[-]	Computational Fluid Dynamics
$C(s)$	[-]	Generic control in the Laplace domain
D	[-]	Differential operator
e_τ	[%]	Relative error on air temperature, T_a
e_Φ	[%]	Relative error on the energy flux, Φ_{abs}
j	[-]	Imaginary unit
$G(s)$	[-]	Generic transfer function in the Laplace domain
$\mathcal{L}$	[-]	Laplace transform operator
K	[N/S]	Static sensitivity of a dynamic system
K_c	[-]	Gain of the control
M_a	[-]	air mass in the plenum chamber
P	[Pa]	pressure of the ideal gas
p_a	[Pa]	pressure of the air in the chamber
P_{a0}	[Pa]	initial value of the air pressure in the chamber
p_i	[-]	I-th pole of the transfer function
R	[$JK^{-1}mol^{-1}$]	Universal constant of gas
s	[-]	Unknown in the Laplace domain
s'	[m]	width of the vertical duct
s''	[m]	width of the U-OWC chamber
T	[s]	Wave period
T_a	[s]	air temperature in the plenum chamber
T_{a0}	[s]	initial value of the air temperature in the plenum chamber
T_{act}	[K]	Actual temperature
T_c	[K]	Output temperature from the control
T_e	[s]	Eigenperiod of the plant
T_i	[s]	Time constant of the ith zero
T_{meas}	[K]	Measured temperature
T_{max}	[K]	Maximum temperature
T_{min}	[K]	Minimum temperature
T_{out}	[K]	Final output temperature
U	[m/s]	water velocity in vertical duct
u_x	[m/s]	horizontal component of U
u_z	[m/s]	vertical component of U
V	[m^3]	volume of the ideal gas
V_a	[m^3]	air volume in the plenum chamber
V_0	[m^3]	initial air volume in the plenum chamber
$X(s)$	[-]	Generic input of a dynamic system in the Laplace domain
$Y(s)$	[-]	Generic output of a dynamic system in the Laplace domain
z_i	[-]	I-th zero of the transfer function

Greek letters

ΔP	[Pa]	Pressure fluctuation
ΔT	[s]	Time step of the CFD simulation
ΔT_a	[K]	variation of the temperature inside the plenum chamber
ΔV_a	[m^3]	variation of the air volume inside the plenum chamber
Φ_{abs}	[W/m]	Energy flux captured by the plant
ϵ	[rad]	phase shift
η	[m]	Free surface elevation
γ	[-]	Exponent of the polytropic law
ζ	[-]	Real constant
σ	[-]	Real part of the Laplace unknown s
$\sigma_{T_{act}}$	[K]	Standard deviation of the actual temperature
$\sigma_{T_{meas}}$	[K]	Standard deviation of the measured temperature
τ	[s]	Time constant of a dynamic system
τ_c	[s]	Time constant of the control
τ_i	[s]	Time constant of the ith pole
τ_{tc}	[s]	Time constant of the thermocouple
ξ	[m]	Free surface elevation inside the chamber
ξ_0	[m]	initial value of ξ
ω	[-]	Imaginary part of the Laplace unknown s
ω_p	[rad/s]	Frequency of the pole
ω_t	[rad/s]	Cutoff frequency of the system
ω_z	[rad/s]	Frequency of the zero

CRediT authorship contribution statement

L. Gurnari: Conceptualization, Formal analysis, Investigation, Methodology, Software, Validation, Writing – original draft, Writing – review & editing. **F. Ruffa:** Conceptualization, Formal analysis, Investigation, Methodology, Writing – original draft. **M. Lugarà:** Investigation, Writing – original draft. **G. Fulco:** Investigation, Writing – original draft. **P. Filianoti:** Conceptualization, Supervision, Validation, Writing – review & editing.

Declaration of competing interest

The authors declare that they have no known competing financial interests or personal relationships that could have appeared to influence the work reported in this paper.

Data availability

No data was used for the research described in the article.

References

[1] B. Czech, P. Bauer, Wave energy converter concepts : Design challenges and classification, IEEE Ind. Electron. Mag. 6 (2) (2012) 4–16, http://dx.doi.org/10.1109/MIE.2012.2193290.

[2] I.López J. Andreu, S. Ceballos, I. Martínez de Alegría, Iñigo Kortabarria, Review of wave energy technologies and the necessary power-equipment, Renew. Sustain. Energy Rev. 27 (2013) 413–434, http://dx.doi.org/10.1016/j.rser.2013.07.009.

[3] B. Drew, A.R. Plummer, M.N. Sahinkaya, A review of wave energy converter technology, Proc. Inst. Mech. Eng., Part A: J. Power Energy 223 (8) (2009) 887–902, http://dx.doi.org/10.1243/09576509JPE782.

[4] T.V. Heath, A review of oscillating water columns, Philos. Trans. R. Soc. 370 (2012) 235–245.

[5] António F. de O. Falcão, Wave energy utilization: A review of the technologies, Renew. Sustain. Energy Rev. 14 (3) (2010) 899–918, http://dx.doi.org/10.1016/j.rser.2009.11.003.

[6] P. Benreguig, J. Kelly, V. Pakrashi, J. Murphy, Wave-to-wire model development and validation for two OWC type wave energy converters, Energies 12 (20) (2019) 3977, http://dx.doi.org/10.3390/en12203977.

[7] A.F.O. Falcão, J.C.C. Henriques, Oscillating-water-column wave energy converters and air turbines: A review, Renew. Energy (ISSN: 0960-1481) 85 (2016) 1391–1424, http://dx.doi.org/10.1016/j.renene.2015.07.086.

[8] A.F. de O. Falc ao, The shoreline OWC wave power plant at the Azores, in: Proc 4th European Wave Energy Conf, Aalborg, Denmark, 2000, pp. 42–47.

[9] T. Heath, T.J.T. Whittaker, C.B. Boake, The design, construction and operation of the LIMPET wave energy converter (Islay, Scotland), in: Proc. 4th European Wave Energy Conf, Aalborg, Denmark, 2000, pp. 49–55.

[10] M. Suzuki, C. Arakawa, S. Takahashi, Performance of wave power generating system installed in breakwater at Sakata port in Japan, in: Proc. 14th Int Offshore Polar Eng Conf, Toulon, France, 2004, pp. 202–209.

[11] T.V. Heath, The development of a turbo-generation system for application in OWC breakwaters, in: Proc. 7th European Wave Tidal Energy Conf, Porto, Portugal, 2007.

[12] Y. Washio, H. Osawa, Y. Nagata, F. Fujii, H. Furuyama, T. Fujita, The offshore floating type wave power device mighty whale: Open sea tests, in: Proc. 10th Int Offshore Polar Eng Conf, Seattle, vol. 1, 2000, pp. 373–380.

[13] P. Boccotti, On a new wave energy absorber, Ocean Eng. 30 (9) (2003) 1191–1200.

[14] P. Boccotti, Caisson breakwaters embodying an OWC with a small opening - Part I: Theory, Ocean Eng. 34 (5–6) (2007) 806–819.

[15] P. Boccotti, Design of breakwater for conversion of wave energy into electrical energy, Ocean Eng. 51 (2012) (2012) 106–118.

[16] P. Boccotti, Wave Mechanics and Wave Loads on Marine Structure, Boston, Butterworth-Heinemann, an Imprint of Elsevier, Amsterdam, 2015.

[17] P. Boccotti, P.G.F. Filianoti, V. Fiamma, F. Arena, Caisson breakwaters embodying an OWC with a small opening - Part II: A small-scale field experiment, Ocean Eng. 34 (5–6) (2007) 820–841.

[18] G. Caprara, L. Martirano, M. Kermani, D. de Mesquita e Sousa, R. Barilli, V. Armas, Cold ironing and battery energy storage system in the Port of Civitavecchia, in: 2022 IEEE International Conference on Environment and Electrical Engineering and 2022 IEEE Industrial and Commercial Power Systems Europe, EEEIC / I & CPS Europe, 2022, pp. 1–6, http://dx.doi.org/10.1109/EEEIC/ICPSEurope54979.2022.9854593.

[19] P. Filianoti, R. Piscopo, Sea wave energy transmission behind submerged absorber caissons, Ocean Eng. 93 (2015) 107–117, http://dx.doi.org/10.1016/j.oceaneng.2014.09.031.

[20] Hsien Hua Lee, Chen-Yen Wen, Guan-Fu Chen, Study on an oscillating water column wave power converter installed in an offshore jacket foundation for wind-turbine system part II: Experimental test on the converting efficiency, Processes 10 (2022) 418, http://dx.doi.org/10.3390/pr10020418.

[21] Fares M'zoughi, Izaskun Garrido, Aitor J. Garrido, Manuel De La Sen, Rotational speed control using ANN-Based MPPT for OWC based on surface elevation measurements, Appl. Sci. 10 (2020) 8975, http://dx.doi.org/10.3390/app10248975.

[22] Salvador Ceballos, Judy Rea, Eider Robles, Iraide Lopez, Josep Pou, Dara O'Sullivan, Control strategies for combining local energy storage with wells turbine oscillating water column devices, Renew. Energy (ISSN: 0960-1481) 83 (2015) 1097–1109, http://dx.doi.org/10.1016/j.renene.2015.05.030.

[23] François-Xavier Faÿ, Ainhoa Pujana, Pablo Ruiz-Minguela, James Kelly, Markus Mueller, João Henriques, Luís Gato, Ana Carrelhas, Bárbara Lopes, Endika Aldaiturriaga, Shoreline OWC wave power plant control algorithms OPERA Project Deliverable, Grant Agreement No 654444.

[24] Bavesh Kooverji, Pneumatic Power Measurement of an Oscillating Water Column Converter, Dissertation Presented for the Degree of Master of Science in Engineering (Mechatronic) in the Faculty of Engineering, Stellenbosch University, 2014.

[25] L. Gurnari, P.G.F. Filianoti, M. Torresi, S.M. Camporeale, 2020 The wave-to-wire energy conversion process for a fixed U-OWC device, Energies 13 (1) (2020) 283.

[26] P. Benreguig, V. Pakrashi, J. Murphy, Assessment of primary energy conversion of a closed-circuit OWC wave energy converter, Energies (2019) http://dx.doi.org/10.3390/en12101962.

[27] R. Suchitra, K. Ezhilsabareesh, A. Samad, Development of a reduced order wave to wire model of an OWC wave energy converter for control system analysis, Ocean Eng. 172 (2019) 614–628.

[28] L. Ciappi, L. Cheli, I. Simonetti, A. Bianchini, L. Talluri, L. Cappietti, G. Manfrida, Analytical models of oscillating water column systems operating with air turbines in the Mediterranean Sea, in: Proceedings of the 15th Conference on Sustainable Development orf Energy, Water and Environment Systems, Cologne, Germany 1–5 September 2020.

[29] Robert Mayon, Dezhi Ning, Chongwei Zhang, Lifen Chen, Rongquan wang - wave energy capture by an omnidirectional point sink oscillating water column system, Appl. Energy (ISSN: 0306-2619) 304 (2021) 117795, http://dx.doi.org/10.1016/j.apenergy.2021.117795.

[30] Lorenzo Cappietti, Irene Simonetti, Valeri Penchev, Philip Penchev, Laboratory tests on an original wave energy converter combining oscillating water column and overtopping devices, in: Guedes Soares (Ed.), in: Advances in Renewable Energies Offshore, © 2019 Taylor & Francis Group, London, ISBN: 978-1-138-58535-5, 2018.

[31] T.S.R. Pereira, T.P. de Carvalho, T.A. Mendes, K.T.M. Formiga, Evaluation of water level in flowing channels using ultrasonic sensors, Sustainability 14 (2022) 5512, http://dx.doi.org/10.3390/su14095512.
[32] Daniel R. David, V. Sundar, S.A. Sannasiraj, Optimizing the opening angle of the harbor wall in an oscillating water column, in: SH - HYDRO 2016 INTERNATIONAL-21st International Conference on Hydraulics, Water Resources and Coastal Engineering 8-10 Dec 2016 Pune, India, 2016.
[33] P. Filianoti, Pulsating flow discharge measurements inside a wave energy converter at sea, in: Proceedings of the 6th IMEKO TC19 Symposium on Environmental Instrumentation and Measurements, Reggio Calabria, Italy, 2016.
[34] Mohammad Shalby, Ahmed Elhanafi, Paul Walker, David G. Dorrell, CFD modelling of a small–scale fixed multi–chamber OWC device, Appl. Ocean Res. (ISSN: 0141-1187) 88 (2019) 37–47, http://dx.doi.org/10.1016/j.apor.2019.04.003.
[35] Weber Jochem, Representation of non-linear aero-thermodynamic effects during small scale physical modelling of oscillating water column wave energy converters, in: Seventh European Wave and Tidal Energy Conference, Porto, Portugal, 2007.
[36] R.P.F. Gomes, J.C.C. Henriques, L.M.C. Gato, A.F.O. Falcão, Testing of a small-scale floating OWC model in a wave flume, in: 4th International Conference on Ocean Energy, 17 October, Dublin.
[37] R.P.F. Gomes, J.C.C. Henriques, L.M.C. Gato, A.F.O. Falcao, Testing of a small-scale floating owc mode in a wave channel and comparison wit numerical results, in: Guedes Soares (Ed.), Renewable Energies Offshore, Taylor & Francis Group, London, 2015, ISBN: 978-1-138-02871-5.
[38] P. Filianoti, S. Camporeale, In field measurements on a small scale OWC device, in: Proceedings of the 8th European Wave and Tidal Energy Conference, Uppsala, Sweden, 7-10 September 2009, ISSN 2309-1983.
[39] M. Shalby, A. Elhanafi, P. Walker, et al., Experimental investigation of the small-scale fixed multi-chamber OWC device, Chin. J. Mech. Eng. 34 (2021) 124, http://dx.doi.org/10.1186/s10033-021-00641-9.
[40] F. Arena, P. Filianoti, Small-scale field experiment on a submerged breakwater for absorbing wave energy, J. Waterway, Port, Coast. Ocean Eng. 133 (2) (2007) 161–167.
[41] P. Filianoti, S.M. Camporeale, A linearized model for estimating the performance of submerged resonant wave energy converters, Renew. Energy 33 (4) (2008) 631–641.
[42] L. Gurnari, P.G.F. Filianoti, S.M. Camporeale, Fluid dynamics inside a U-shaped oscillating water column (OWC): 1D vs. 2d CFD model, Renewable Energy 193 (2022) (2022) 687–705.
[43] P. Filianoti, L. Gurnari, The performance of an active submerged breakwater by a cfd analysis, in: Proceedings of the International Offshore and Polar Engineering Conference, 2019, vol. 3, 2019, pp. 3702–3705.
[44] R.G. Dean, R.A. and Dalrymple, Water Wave Mechanics for Engineers and Scientists, Prentice Hall, Inc. Reprinted Singapore: World Scientific Publishing Co. 1991, 1984, pp. 170–178, [a] Neubert H.K.P., Instrument Transducers – An Introduction to their Performance and Design, Page: 319.
[45] H.K.P. Neubert, Instrument Transducers: An Introduction To their Performance and Design, Clarendon Press, ISBN: 9780198563204, 1975.
[46] J.P. Holman, Experimental Methods for Engineers, seventh ed., McGraw-hill, New York, 2001.
[47] R.S. Figliola, D.E. Beasley, Theory and Design for Mechanical Measurements, Wiley, New York, 1991.
[48] Omega Technologies Handbook, Thermocouple Reference Tables, Omega EngineeringInc., 1993, p. B172.
[49] R.P. Benedict, P.E, Fundamentals of Temperature, Pressure, and Flow Measurements, third ed., John Wiley & Sons, New York, 1984.
[50] T.D. McGee, Principles and Methods of Temperature Measurements, John Wiley & Sons, New York, 1988.
[51] T.W. Kerlin, Industrial Temperature Measurement, Instrument Society of America, Research Triangle Park, N.C., 1982.
[52] J.W. Murdock, C.J. Foltz, C. Gregory, A practical method of determining response time of thermometers in liquid baths, J. Eng. Power (1963).
[53] J. Yin, M.K. Jensen, Analytic model for transient heat exchanger response, Int. J. Heat Mass Transfer 46 (2003).
[54] B. Serio, Ph. Nika, J.P. Prenel, Static and Dynamic Calibration of Thin-Film Thermocouples By Means of a Laser Modulation Technique, American Institute of Physics, 2000.
[55] H. Niemann, R. Miklos, A simple method for estimation of parameters in first order systems, J. Phys. Conf. Ser. 570 (1) (2014).
[56] E.O. Doebelin, System Dynamics: Modeling, Analysis, Simulation, Design, CRC Press, ISBN: 9780824701260.
[57] F.P. Incropera, D.P. DeWitt, Introduction to Heat Transfer, Wiley, ISBN: 0471304581.